Design of a Microelectronic Neurobridge Device for the Paralyzed Limbs and Motor Function Reconstruction

Kun Liu[1], Jieshu Gao[2*]

ABSTRACT

To reconstruct the motor and sensory functions of human following brain nerve injury, we design a microelectronic neurobridge device as a replacement for the impaired brain nervous tissues. The sensory and motor functions are reconstructed for the paralyzed limbs. Models of this system are established along with the motor nerve signal detection device, signal acquisition device, microelectronic neurobridge testing machine, fast algorithm validation platform and action potential detection and recognition circuit. To solve the problem of low accuracy in detecting action potentials, we propose the core algorithm for the microelectronic neurobridge. This algorithm is based on constraints on amplitude thresholds and differential thresholds, and the time domain features are considered. The type feature vectors are obtained by K-means clustering with higher sensitivity and specificity. Real-time detection and processing of signals are achieved by using real-time fast algorithm. Human hand movement is detected by the double-channel microelectronic neurobridge device. Our findings provide a new solution to restore the motor functions of paralyzed patients.

Key Words: Paralysis, Brain Nerve Injury, Microelectronic Neurobridge, Action Potential Detection, Motor Function Reconstruction

DOI Number: 10.14704/nq.2018.16.2.1180 **NeuroQuantology 2018; 16(2):75-82**

Introduction

Paralysis, defined as a complete or partial loss of tactile and motor functions of muscles due to brain nerve injury, has already become a global medical concern. Figure 1 shows the age distribution of paralyzed people released by an authority. The peak onset age of paralysis is 40 to 59 years old, accounting for about 48%. Those with paralysis and aged above 60 years old account for 32%. The average age of paralyzed people is 51 years old (Gao *et al.,* 1997).

Paralysis is mainly caused by cerebral stroke (Rakusa *et al.,* 2014). Brain nerve cells have limited regenerative ability, and the brain nerve injury will damage the environment for the generation of the nerve cells, leading to paralysis (Dobkin, 2000). Study has shown that neuroglian and myelin proteins are key factors inhibiting the regeneration of nerve cells at an early stage following brain nerve injury. Astroglia is the primary factor inhibiting the regeneration of nerve cells at a later stage following brain nerve injury (Hansson and Brismar, 2003). Paralysis is mainly caused by cerebral stroke (Rakusa *et al.,* 2014).

Brain nerve cells have limited regenerative ability, and the brain nerve injury will damage the environment for the generation of the nerve cells, leading to paralysis (Dobkin, 2000). Study has shown that neuroglian and

Corresponding author: Jieshu Gao
Address: [1]School of Information Engineering, Qujing Normal University, Qujing 655011, China; [2]YingKou Institute of Technology, Yingkou 115000, China
e-mail ✉ gaojieshu@sina.com.cn
Relevant conflicts of interest/financial disclosures: The authors declare that the research was conducted in the absence of any commercial or financial relationships that could be construed as a potential conflict of interest.
Received: 9 January 2018; **Accepted:** 11 February 2018

myelin proteins are key factors inhibiting the regeneration of nerve cells at an early stage following brain nerve injury. Astroglia is the primary factor inhibiting the regeneration of nerve cells at a later stage following brain nerve injury (Hansson and Brismar, 2003).

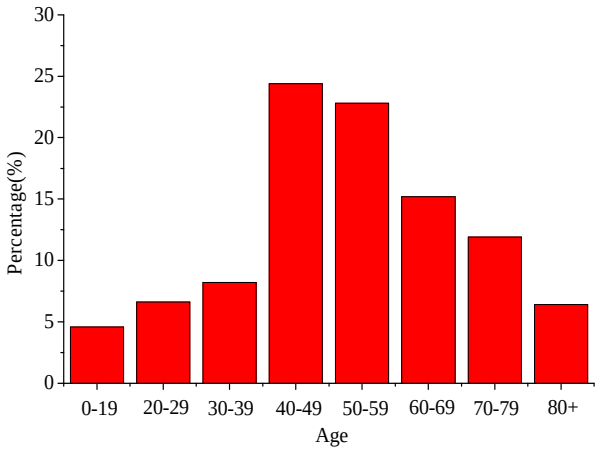

Figure 1. Age distribution map of paralyzed patients

How to reconstruct the motor and sensory functions following brain nerve injury is among the major difficulties in paralysis research and treatment (Moskowitz, 1989). For the repair of the nervous system, advances in biomedicine, cardiac pacemaker and artificial retina are utilized, and some progress has been made in local motor and sensory reconstruction (Marqueste *et al.,* 2004).

Microelectronic neurobridge is the new nerve signal and transmission technique developed in recent years (Björkman *et al.,* 2005). Neurobridge device is based on microcomputer and receives and transmits the central nervous system signals in place of the impaired brain nerves. It is considered as a paralysis treatment system with a broad prospect (Almli and Stanley., 1992; Kemp *et al.,* 2015).

We propose a microelectronic neurobridge device for motor and sensory reconstruction following brain nerve injury. This system can fulfil the functions that are once performed by the brain nerves. Our research sheds new light on the reconstruction of motor function for paralyzed patients.

Microelectronic neurobridge device

We propose a microelectronic neurobridge device for nerve signal reconstruction and transmission following brain nerve injury (Gale & Prigatano, 2010; Ewan and Martin, 2011). The general architecture of the neurobridge device is shown in Figure 2.

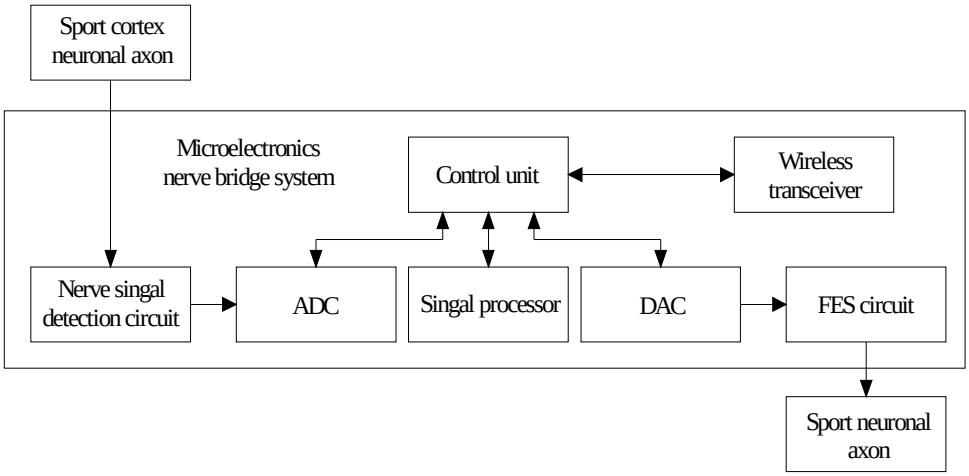

Figure 2. Block diagram of microelectronics nerve bridge system

The nerve signal detection device is placed in the neuronal axon of motor cortex to detect action potentials. The signals are denoised, filtered and amplified before analog-to-digital conversion (ADC). Then the converted signals are input into the signal processor (Pruitt *et al.,* 2016; Hokfelt *et al.,* 1998; Banati *et al.,* 2001). The core algorithm of the neurobridge device is the human action detection algorithm. The calculation results are feedback into the central controller. The system has a wireless receiver that enables offline computation. The results are converted into excitation waveforms via DAC. Finally, the excitation waveforms are converted into current output signals by functional electrical stimulation. These signals will stimulate the motor neuronal axons, inducing the generation of action potentials.

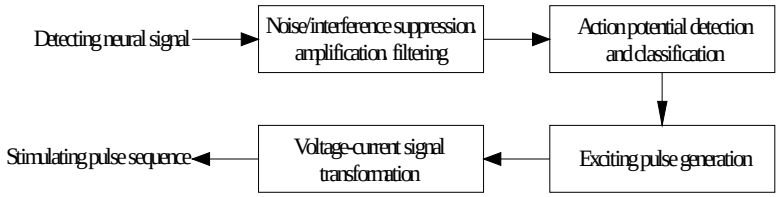

Figure 3. Flow chart of microelectronics nerve bridge data processing

Figure 3 is the flow chart of data processing in the microelectronic neurobridge. The raw signals are small in amplitude and contaminated by noises. Low-frequency noises cause drift and boundary mutation of raw signals. The signal detection device is responsible for denoising, amplifying and filtering of the raw signals, thus increasing the signal-to-noise ratio (SNR) and inhibiting low frequency drift. Raw signals contain several action potentials. It is

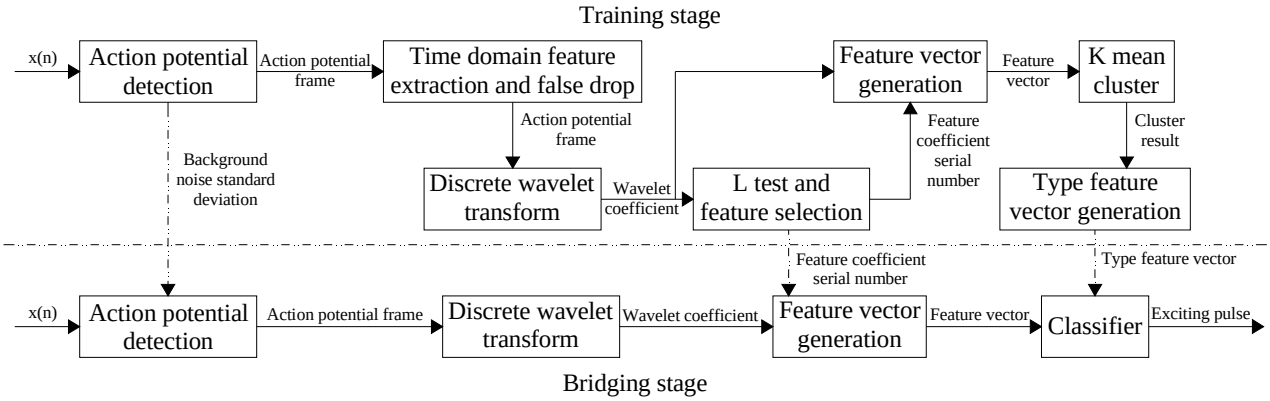

Figure 4. Data processing flow of training stage and bridging stage

necessary to identify the action potentials produced by the neurons through detection and separation algorithms so as to generate excitation pulses.

Algorithms of the microelectronic neurobridge

Action potential detection and classification are first analyzed. Data processing in microelectronic neurobridge mainly consists of two parts, training and bridging, as shown in Figure 4. Training can be done offline or online, while bridging must be done online.

First the simulation data are input for the training. Attenuation factor is introduced to inhibit waveform mutation of the potential sequences:

$$x'(n)=\begin{cases} x(n), 0 < n \geq 54 \\ x(n)\cdot e^{-(n-54)/2}, 54 \leq n \leq 64 \\ 0, n = 65 \end{cases} \quad (1)$$

$x(n)$ and $x'(n)$ are the data before and after adjustment, respectively. Before computation, estimation and elimination of environmental noises are performed first. Function H(m, h) is defined as follows:

$$H(m,h)=\begin{cases} 1, R(x(n)) < Rthr, n \in (m-h, m+h) \\ 0, R(x(n)) \geq Rthr, n \in (m-h, m+h) \end{cases} \quad (2)$$

R(X) is the range of $x(n)$:

$$R(x(n)) = \max(x(n)) - \min(x(n)) \quad (3)$$

Rthr is the threshold for R(X). Standard deviation for noise estimation is represented as

$$\sigma_n(m,h)=\begin{cases} median\left\{\frac{|x(n)|}{0.6745}\right\}, n \in (m-h, m+h), H(m,h)=1 \\ 0, n \in (m-h, m+h), H(m,h)=0 \end{cases} \quad (4)$$

Where m is the central coordinate, and h is the radius. Figure 5 shows the standard deviations for noise estimation by using the proposed method, conventional algorithm and future value algorithm. The noise signals used for the calculation obey a normal distribution. As the discharge frequency gradually increases, the error increases for each algorithm, and the increase amplitude is the greatest with the conventional algorithm. When the discharge frequency increases to 100Hz, the error with the conventional algorithm is 68%; that of the future value algorithm is 10.5%, while our proposed algorithm has an error of only about 2.6%.

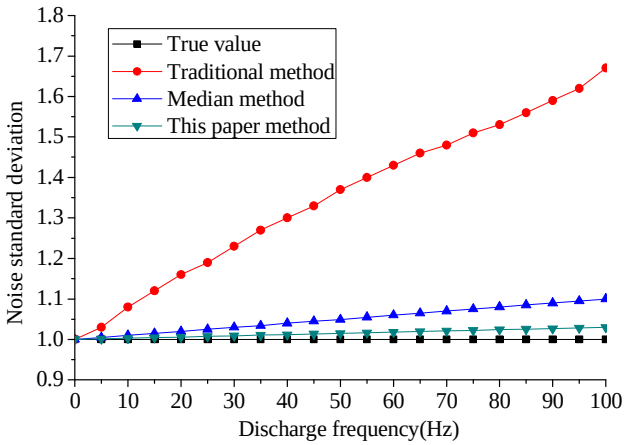

Figure 5. Comparison of different estimation methods

Detection of action potential:

$$\varphi\left(x\left(t\right)\right)=\left(dx\left(t\right)/dt\right)^{2}-x\left(t\right)\left(d^{2}x\left(t\right)/dt^{2}\right) \quad (5)$$

Where $x(t)$ is the detection signals, and φ is the non-linear operator. Formula (2) detects action potential by instantaneous frequency and instantaneous amplitude. The detection result is better at a lower SNR. The time domain features are extracted. Feature vectors are generated by wavelet transform, and type feature vectors are obtained by K-means clustering. The algorithm used for bridging is similar to that used for training.

Actual detection is usually influenced by environmental noises. The detection is usually evaluated by the omission rate and false detection rate. Let N_n and N_t be the number of action potentials omitted and the actual number of action potentials, respectively; and N_p and N_d be the number of action potentials falsely detected and the number of action potentials using the amplitude threshold algorithm, respectively. Thus, the sensitivity S_n and specificity S_p of one algorithm in action potential detection are respectively given as follows:

$$S_{n}=1-\frac{N_{n}}{N_{t}},S_{p}=1-\frac{N_{p}}{N_{d}} \quad (6)$$

The larger the S_n, the better the detection effect and the smaller the N_n; the larger the S_p, the lower the false detection rate.

Conventional amplitude threshold algorithm exhibits a higher sensitivity at the expense of S_p. In other words, false detections are more frequent using the conventional amplitude threshold algorithm. We have made certain modifications on the basis of the conventional amplitude threshold algorithm, and the formula for the threshold algorithm is written below:

$$\begin{cases} x\left(i\right)\geq Thr, x\left(i-1\right)<Thr \\ x\left(i\right)-x\left(i-1\right)>\dfrac{a}{\sigma_{n}} \end{cases} \quad (7)$$

where Thr is the threshold; σ_n is the standard deviation of noise estimation; a is correlation coefficient.

Actual action potentials are detected using the proposed threshold algorithm, as shown in Table 1. The improved algorithm has a higher sensitivity, whose average is 99.39%. S_p increases dramatically, with an average of 96.28%, which verifies the validity and superiority of the proposed algorithm.

Sixteen datasets are used. Action potentials are detected using the conventional algorithm and the proposed algorithm, respectively, and the values of S_n and S_p using the two algorithms are shown in Fig. 6. Compared with conventional algorithm, our proposed algorithm has a great increase in sensitivity, while the specificity is generally maintained above 94%.

K-means clustering is applied to the action potentials detected above. Clustering can differentiate the action potentials produced by different neurons and extract the features for the same type of potentials. For the K-means clustering, the criterion function is expressed as follows:

$$J_{j}=\sum_{i=1}^{n_{j}}\left\|X_{i}^{j}-Z_{j}\right\|^{2} \quad (8)$$

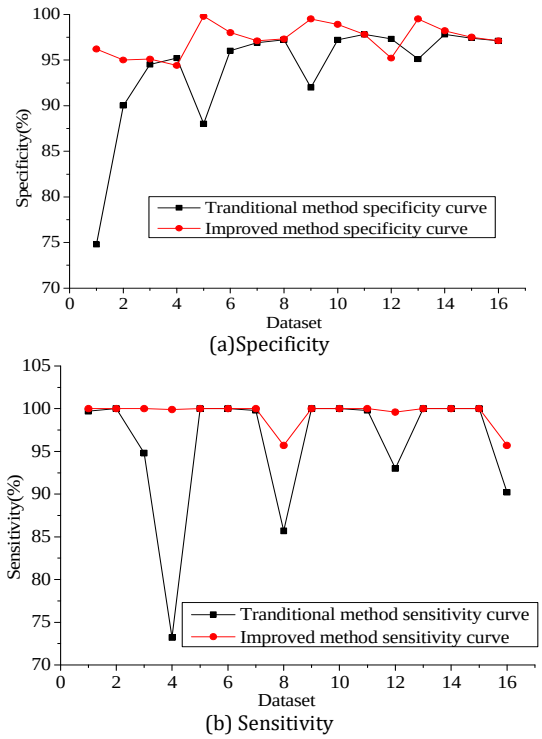

Figure 6. Comparison of two methods

Where n_j is the sample size; X_i^j is the feature vector of the sample; Z_j is the cluster center. The set J of all criterion functions is

$$J = \sum_{j=1}^{c} J_j = \sum_{j=1}^{c} \sum_{i=1}^{n_j} \left\| X_i^j - M_j \right\|^2 \quad (9)$$

Partial derivative is taken of formula (9):

$$\frac{\partial}{\partial Z_j} \sum_{i=1}^{n_j} \left\| X_i^j - Z_j \right\|^2 = \frac{\partial}{\partial Z_j} \sum_{i=1}^{n_j} \left(X_i^j - Z_j \right)^T \left(X_i^j - Z_j \right) = 0 \quad (10)$$

Let x and y be the feature vectors of the sample to be calculated. Using Euclidean distance $D_O(x, y)$ and Mahalanobis distance $D_M(x, y)$, the similarity measure of feature vector is calculated:

$$D_O(x, y) = \sqrt{(x_1 - x_2)^2 + (y_1 - y_2)^2} \quad (11)$$

$$D_M(x, y) = \sqrt{(x - y)' \Sigma^{-1} (x - y)} \quad (12)$$

Table 2 shows the accuracy of action potential detection using K-means clustering, along with the calculated results of $D_O(x, y)$ and $D_M(x, y)$.

Table 1. Improved detection results of amplitude threshold algorithm in action potentials

Data set	Noise standard deviation	Total action potential	Undetected number	False drop number	Sensitivity %	Specificity %
1	0.05	3523(780)	0(188)	119	100	96.12
	0.10	3530(771)	0(179)	180	99.81	95.27
	0.15	3479(785)	0(217)	171	100	95.83
	0.20	3486(783)	5(224)	202	100	93.96
2	0.05	3416(788)	0(209)	13	100	98.29
	0.10	3517(819)	0(224)	68	99.38	98.35
	0.15	3418(766)	1(230)	96	97.26	98.01
	0.20	3533(814)	103(287)	89	100	97.42
3	0.05	3387(773)	0(234)	24	100	99.54
	0.10	3450(805)	0(233)	49	100	96.75
	0.15	3465(817)	0(242)	80	100	96.94
	0.20	3428(782)	18(267)	153	99.31	96.17

Table 2. Normality test of characteristic parameter selecting +K means clustering results

Dataset	Noise standard deviation	Action potential	European distance measure		Ma's distance measure	
			Total errors	Correct rate	Total errors	Correct rate
1	0.05	3280(551)	0(15)	99.54%	0(15)	99.54%
	0.10	3354(556)	0(17)	99.62%	0(17)	99.62%
	0.15	3203(541)	0(27)	99.13%	0(27)	99.13%
	0.20	2612(489)	4(68)	98.39%	3(68)	98.24%
2	0.05	3194(572)	0(3)	99.88%	0(3)	99.88%
	0.10	3278(587)	45(4)	97.26%	0(4)	97.26%
	0.15	3137(544)	17(23)	96.73%	0(23)	96.73%
	0.20	2099(415)	814(28)	49.87%	5(28)	97.38%
3	0.05	3130(522)	0(0)	100%	0(0)	100%
	0.10	3234(579)	60(4)	97.17%	0(4)	98.29%
	0.15	3185(564)	352(13)	88.26%	0(13)	98.36%
	0.20	2456(457)	670(33)	66.35%	0(33)	97.93%
4	0.05	3206(589)	11(1)	98.45%	0(1)	99.49%
	0.10	3276(520)	234(5)	90.74%	0(5)	92.55%
	0.15	3050(577)	525(4)	84.73%	4(4)	95.68%
	0.20	2332(388)	646(6)	68.84%	25(6)	99.88%

As seen from the table above, the effect of clustering based on $D_M(x, y)$ is better than based on $D_O(x, y)$. Since the number of dimensions in the features extracted using the probability density function is small, every feature vector has several wave peaks. Thus under considerable environmental noises, the clustering effect is better based on $D_M(x, y)$.

Reconstruction of motor function using microelectronic neurobridge for paralyzed patients

Figure 7 shows the schematic for reconstructing the motor function for patients with cerebral palsy using microelectronic neurobridge. The nerve signals produced by the brain nerve system cannot be transmitted to the affected limbs, so the motor signals in the healthy limbs are detected using the microelectronic neurobridge device. These signals are converted into electrical stimulation signals through relevant algorithms, which are then applied to the affected limbs. In this way, the motor function is reconstructed.

Detection circuit for motor signals is expressed as:

$$G_{max} = 20\log\left(\frac{3}{0.001}\right) = 69.54\text{dB} \quad (13)$$

$$G_{min} = 20\log\left(\frac{3}{\frac{1}{2}\cdot 2^{12}\cdot 10^{-6}}\right) = 63.32\text{dB} \quad (14)$$

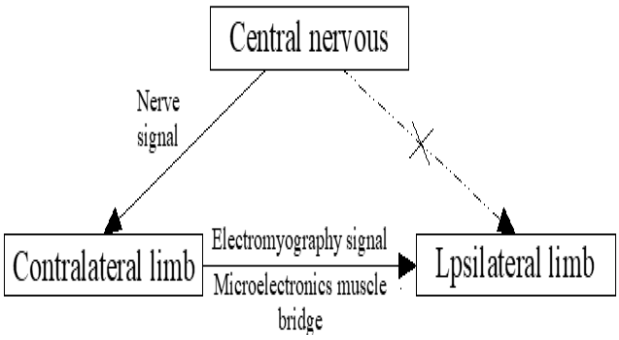

Figure 7. Diagram of microelectronics muscle bridge based on stroke movement function reconstruction

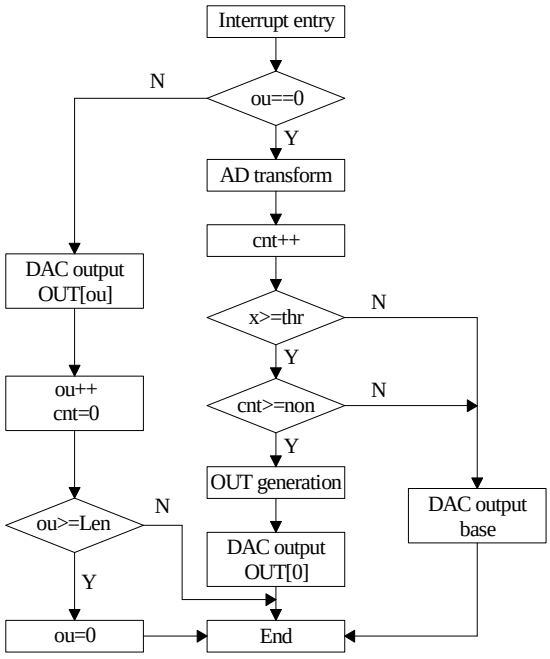

Figure 8. Flow chart of algorithm hardware program

Figure 8 shows the flow chart of algorithms used in microelectronic neurobridge. OUT is the repository of excitation waveforms; ou is the explanation of the output status; Thr is the threshold for electromyographic signals; cnt is the counter; x is the value after the conversion of electromyography (EMG) signals; Len is the length of OUT. Following the flow chart in Fig. 8, the surface EMG signals and the excitation pulse signals are output and used for strength testing.

The subjects were males, physically healthy and aged 20-27 years old. The subjects sat straight on chairs, with the right arm on the armrest and the right wrist suspended. Different static loads were imposed on the right wrist, and the tests were performed for five times. After each test, the subjects took a rest for 5min before the next test. Fig. 9 shows the curves of maximal volitional contraction (MVC) and stimulation frequency (SF) under different thresholds for electrical signals for two volunteers. Polynomial fitting was performed using the scattered values. The degree of linearity is expressed as follows:

$$L = \frac{\Delta SF_{max}}{SF_{max} - SF_{min}} \times 100\% \quad (15)$$

The larger the L, the lower the degree of linearity. As seen from the figure, the larger the MVC, the larger the SF. Generally, MVS squared is linearly related to SF. Besides, when Thr=0.07, SF

under the same MVC is smaller than that when Thr=0.1. As analyzed above, the value of Thr should be properly adjusted for different positions of the human body, so as to improve the detection of motor signals.

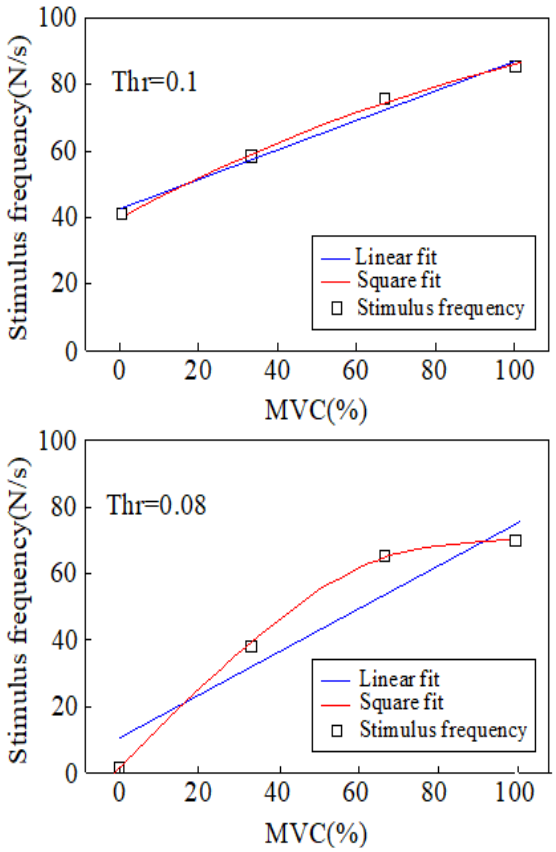

Figure 9. Performance of single channel excitation pulse generating algorithm

Conclusion

We establish a microelectronic neurobridge device to reconstruct the motor and sensory functions following brain nerve injury. This system can act as a substitute for the injured brain nerve cells. Our research offers a new solution for reconstructing the motor function for paralyzed patients.

Models of this system are established along with the motor nerve signal detection device, signal acquisition device, microelectronic neurobridge testing machine, fast algorithm validation platform and action potential detection and recognition circuit. To solve the problem of low accuracy in detecting action potentials, we propose the core algorithm for the microelectronic neurobridge. This algorithm is based on constraints on amplitude threshold and differential threshold and considers the time domain features. The type feature vectors are obtained by K-means clustering with higher sensitivity and specificity. Real-time detection and processing of signals are achieved by using real-time fast algorithm. Human hand movement is detected by the double-channel microelectronic neurobridge.

To solve the problem of low accuracy in detecting action potentials, we propose the core algorithm for the microelectronic neurobridge. This algorithm is based on constraints on amplitude threshold and differential threshold and considers the time domain features. The type feature vectors are obtained by K-means clustering with higher sensitivity and specificity. Real-time detection and processing of signals are achieved by using the real-time fast algorithm. Human hand movement is detected by the double-channel microelectronic neurobridge device.

References

Almli C, Finger S. Brain injury and recovery of function: theories and mechanisms of functional reorganization. Journal of Head Trauma Rehabilitation 1992; 7(2): 70-77.

Banati RB, Cagnin A, Brooks DJ, Gunn RN, Myers R, Jones T. Long-term trans-synaptic glial responses in the human thalamus after peripheral nerve injury. Neuroreport 2001; 12(16), 3439-42.

Björkman A, Rosén B, Lundborg G. Enhanced function in nerve-injured hands after contralateral deafferentation. Neuroreport 2005;16(5):517-19.

Dobkin BH. Functional rewiring of brain and spinal cord after injury: the three Rs of neural repair and neurological rehabilitation. Current Opinion in Neurology 2000;13(6):655-9.

Ewan EE, Martin TJ. Rewarding Electrical Brain Stimulation in Rats after Peripheral Nerve InjuryDecreased Facilitation by Commonly Abused Prescription Opioids. Anesthesiology: The Journal of the American Society of Anesthesiologists 2011; 115(6):1271-80.

Gale SD, Prigatano GP. Deep white matter volume loss and social reintegration after traumatic brain injury in children. Journal of Head Trauma Rehabilitation 2010; 25(25): 15-22.

Gao H, Qiao X, Hefti F, Hollyfield JG, Knusel B. Elevated mRNA expression of brain-derived neurotrophic factor in retinal ganglion cell layer after optic nerve injury. Investigative Ophthalmology & Visual Science1997;38(9):1840-47.

Hansson T, Brismar T. Loss of sensory discrimination after median nerve injury and activation in the primary somatosensory cortex on functional magnetic resonance imaging. Journal of Neurosurgery 2003; 99(1): 100-05.

Hokfelt T, Broberger C, Diez M, Zhang X, Kopp J, Xu ZQ, Landry M, Bao L. Neuropepide Y and its receptors in brain diseases and after nerve injury. European Neuropsychopharmacology 1998; 8: S84-85.

Kemp SW, Szynkaruk M, Stanoulis KN, Wood MD, Liu EH, Willand MP, Morlock L, Naidoo J, Williams NS, Ready JM, Mangano TJ. Pharmacologic rescue of motor and sensory function by the neuroprotective compound P7C3 following neonatal nerve injury. Neuroscience 2015; 284:202-16.

Levin HS, Wilde EA, Chu Z, Yallampalli R, Hanten GR, Li X. Diffusion tensor imaging in relation to cognitive and functional outcome of traumatic brain injury in children. Journal of Head Trauma Rehabilitation 2008; 23(4): 197-208.

Marqueste T, Alliez JR, Alluin O, Jammes Y, Decherchi P. Neuromuscular rehabilitation by treadmill running or electrical stimulation after peripheral nerve injury and repair. Journal of Applied Physiology 2004; 96(5): 1988-95.

Moskowitz E. Peripheral nerve lesions in traumatic brain-injured patients. American Journal of Physical Medicine & Rehabilitation 1989; 68(5): 256-64.

Pruitt DT, Schmid AN, Kim LJ, Abe CM, Trieu JL, Choua C, Hays SA, Kilgard MP, Rennaker RL. Vagus nerve stimulation delivered with motor training enhances recovery of function after traumatic brain injury. Journal of neurotrauma 2016;33(9):871-79.

Rakusa M, Gak S, Alekseenko Y, Ehler E, Muresanu D, Opara J, Vos P. Can young European neurologists comfortably manage patients with traumatic brain, spine or nerve ınjuries (TBI)? Neurology 2014; 82(10 Supplement): P1-309.